Proceedings of the 9th U.S. National and 10th Canadian Conference on Earthquake Engineering
Compte Rendu de la 9ième Conférence Nationale Américaine et
10ième Conférence Canadienne de Génie Parasismique
July 25-29, 2010, Toronto, Ontario, Canada • Paper No 1188

SEISMIC BEHAVIOR OF HIGH-PERFORMANCE FIBER-REINFORCED CONCRETE BRIDGE PIERS

A. Aviram[1] , B. Stojadinovic[2], and G. Parra-Montesinos[3]

ABSTRACT

An experimental and analytical study was carried out on two circular column specimens representing cantilever bridge piers constructed with tensile strain-hardening, high-performance fiber-reinforced concrete. The approximately ¼-scale specimens reinforced with a 1.5% volume fraction of high-strength hooked steel fibers, relaxed transverse reinforcement, and different longitudinal reinforcement details for the plastic hinge zone, were subjected to cyclic bidirectional lateral displacements. The cyclic behavior and damage tolerance at various drift levels were compared to those for a geometrically "identical" specimen constructed using regular concrete and designed according to current Caltrans bridge design specifications. The bridge columns were modeled in OpenSees finite-element program using a distributed-plasticity fiber model. The experimental and analytical results demonstrate the considerable benefits of this type of fiber-reinforced concrete for use in typical highway overpass bridges, i.e. substantial reduction in transverse reinforcement, improved cyclic response, and increased damage tolerance, with the associated construction benefits and potential reductions in post-earthquake repairs.

Introduction

Numerous structures worldwide, including precast and cast-in-place reinforced concrete infrastructure systems, suffered significant damage or collapse during historical and recent earthquakes (1971 San Fernando, USA; 1989 Loma Prieta, USA; 1994 Northridge, USA; 1995 Kobe, Japan; 1999 Kocaeli, Turkey; 1999 Chi-Chi, Taiwan; etc.), primarily due to deficient structural design. On the other hand, reinforcement detailing required to ensure adequate seismic behavior of critical bridge and building members often lead to substantial reinforcement congestion and construction difficulties. Therefore, it is not surprising that many recent research efforts have been directed to the development and implementation of innovative materials in new structures to enhance their seismic performance while reducing required reinforcement detailing.

In the past few years, fiber-reinforced concretes (FRCs) with a relatively low fiber volume fraction (V_f=1.5-2.0%) that exhibit a tensile strain-hardening behavior and a compression response that resembles that of well-confined concrete have become available. Hooked and

[1]Ph.D. Candidate, Dept. of Civil and Environmental Eng., University of California, Berkeley CA 94720-1710
[2]Professor, Dept. of Civil and Environmental Eng., University of California, Berkeley CA 94720-1710
[3]Associate Professor, Dept. of Civil and Environmental Eng., University of Michigan, Ann Arbor, MI 48109-2125

twisted steel fibers, as well as ultra high molecular weight polyethylene fibers, are among the typical fibers used (Parra-Montesinos, 2005). This new class of FRC, referred to as high-performance FRC (HPFRC), is considered to be tougher and is thought to be more durable than traditional FRCs. When used in structural elements subjected to large displacement reversals, HPFRCs have led to significant deformation capacity with superior damage tolerance compared to regular reinforced concrete members (Yoon *et al.* 2002; Harajli and Rteil 2004; Parra-Montesinos 2005; Canbolat *et al.* 2005; Cheng and Parra-Montesinos 2007; Parra-Montesinos and Chompreda 2007). Further, substantial reductions in transverse reinforcement required for confinement and shear resistance have been possible in elements subjected to large shear stress reversals (Parra-Montesinos, 2005). The enhanced structural properties of these HPFRC members indicate that HPFRC materials have great potential for use in flexural elements subjected to large drift demands during ground motions, such as bridge piers with either flexural-dominated behavior or with strong flexure-shear interaction.

The use of HPFRC in the construction of bridge piers, to substantially relax transverse reinforcement requirements while leading to increased damage tolerance, shear strength, and energy dissipation under cyclic loading in comparison to regular concrete piers, is the main focus of this paper. An experimental and analytical study was carried out on two approximately ¼-scale column specimens built with HPFRC and the behavior compared with that of a geometrically "identical" conventionally-reinforced concrete (RC) column tested by Terzic *et al.* (2008). A comparison of the quasi-static bi-directional cyclic test results of the HPFRC and conventional RC specimens is presented in this paper. Additional information about the tests, calibrated finite element models, as well as the repair cost and time analysis of typical highway bridges in California constructed using these two column designs can be found elsewhere (Aviram, 2009).

Experimental Test Procedure

The circular column specimens, representing approximately ¼-scale cantilever bridge piers, were constructed with an HPFRC material reinforced with a 1.5% volume fraction of commercially available high-strength (350 ksi) hooked steel fibers with a length of 1.2" and an aspect ratio of 80. The columns were detailed with modified longitudinal reinforcement for the plastic hinge zone and relaxed transverse reinforcement compared to the Caltrans Seismic Design Criteria (SDC) (2004) for regular concrete bridge columns, utilizing the enhanced shear strength provided by the steel fibers. Ready-mix concrete was used in both columns and the fibers were added to the concrete truck on site. HPFRC casting was performed using a bucket and stick vibrator. The column specimens represent the bottom half of a typical bridge column deforming in double curvature with an assumed inflection point at mid-height. The column base was connected to a massive reinforced concrete anchor block, simulating fixed boundary conditions.

Table 1 presents the main geometric and reinforcement characteristics of the three column specimens compared in this study: Specimen 1 (S1) and Specimen 2 (S2) built with HPFRC, and the reference base column (BC) built with regular concrete and tested by Terzic *et al.* (2008). Because no fibers crossed the cold joint between the concrete base and the HPFRC column, dowel reinforcement was added at the column base of Specimens S1 and S2 to prevent concentration of rotations and force inelastic deformations to occur slightly above the column base. Two reinforcement details in the plastic hinge region were evaluated. In Specimen S1, the

upper portion of the dowels was debonded through the use of plastic tubes in order to avoid premature damage localization that could occur because of the termination of the bars within the plastic hinge zone. In Specimen S2, the dowels were terminated within the plastic hinge region and the main longitudinal bars were debonded over a length of 4 in. in order to prevent strain concentration and premature rebar fracture in the section were the dowels are terminated. The reinforcement details for the two HPFRC specimens are shown in Figure 1.

Table 1. Summary of geometric and reinforcement details of HPFRC and regular concrete column specimens.

Parameter	S1: HPFRC	S2: HPFRC	BC: Plain
D_{col} – Column diameter	16”	16”	16”
H_{col} – Total col. height	64”	64”	64”
Shear span-diameter ratio	4	4	4
Long. reinf.	12#4+8#4 dowels	12#4+8#4 dowels	12#4
ρ_l – Long. reinf. ratio	2% (base), 1.2% (rest)	2% (base), 1.2% (rest)	1.2%
Debonding sleeves	Dowels, L = 10”, H_{bot}* = 10”	Main rebar, L = 4”, H_{bot} = 8”	-
Transv. reinf.	W3.5**@2.5”	W3.5@2.5”	W3.5@1.25”
ρ_s – Transv. reinf. ratio	0.75%	0.75%	1.5%
f'_c- Conc. compr. strength	6.86 ksi	6.86 ksi	5.09 ksi

*H_{bot} = Length of longitudinal rebar between the foundation level and debonded region.
**W3.5: Diameter = 0.21 in.

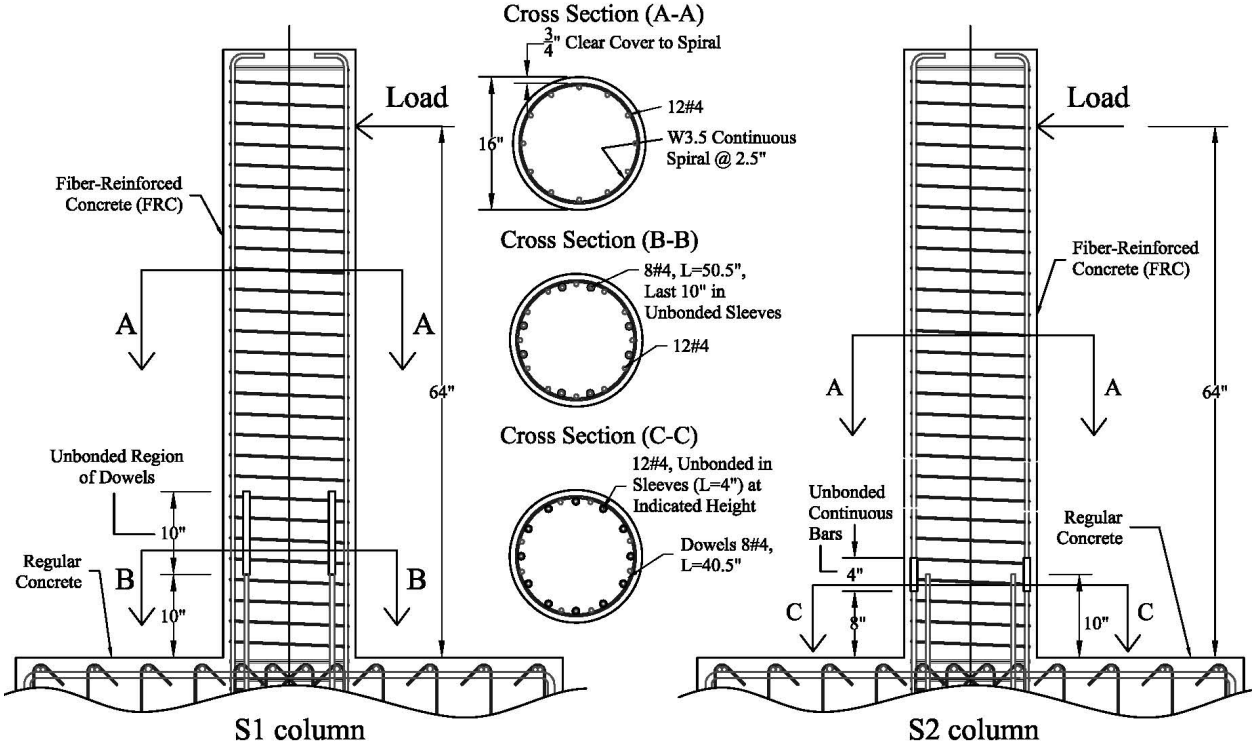

Figure 1. Reinforcement detailing of HPFRC specimen

A circular load pattern, applied using two actuators at an initial 90° angle with respect to each other, was defined for the bidirectional quasi-static cyclic test of the HPFRC column specimens, similar to that used by Terzic *et al.* (2008) for the BC cyclic test. The quasi-static

cyclic tests were conducted by incrementally increasing the radius of the circular pattern, defined by two circular cycles at each displacement level, one clock-wise and the other counter-clock-wise. This load pattern was selected to minimize the bias in column damage in any particular direction; however, it results in a highly demanding displacement history on the column. Special care was taken when developing the loading pattern as to exclusively induce lateral displacement and no torsion in the column, accounting for second-order specimen geometry effects and actuator elongations. The target displacement ductility demand for each complete cycle in the displacement history is presented in Table 2. The ductility demand was computed with respect to the BC column yield point, estimated at 0.55", to enable a direct comparison between the BC and HPFRC specimens by applying the same drift demands. In the post-yield displacement history, each main cycle or displacement level was followed by a small displacement cycle equal to one-third of the primary cycle (maximum drift applied up to that point) to evaluate the column stiffness degradation throughout the loading history. A gravity load equivalent to 10% of the axial capacity of the BC column was applied to the column top through a spreader beam and hydraulic jacks.

The maximum ductility level attained during the test of the reference column BC was 4.5 (3.9% drift ratio). The tests of HPFRC column tests were extended beyond ductility 4.5 using the increment pattern shown in Table 2. The maximum ductility level attained during the test of the S1 and S2 columns without substantial loss of gravity load carrying capacity was 12.5 and 6.25, respectively (10.7 and 5.4% drift ratio). Due to different locations of the plastic hinge and slightly larger yield curvature caused by different material strengths and presence of dowels, the displacement history imposed on HPFRC specimens corresponds to different column ductility and plastic hinge rotation demands than those for the BC column, as shown in Table 2.

Table 2. Nominal ductility level used at each cycle of the displacement history, defined with respect to the BC column yield displacement.

Cycle	Ductility level	Displ., in (Drift, %)	Cycle	Ductility level	Displ., in (Drift, %)
1	0.08	0.04 (0.07)	10	3	1.65 (2.58)
2	0.2	0.11 (0.17)	11	1	0.55 (0.86)
3	0.4	0.22 (0.34)	12	4.5	2.48 (3.87)
4	1	0.55 (0.86)	13	1.5	0.83 (1.29)
5	0.33	0.18 (0.28)	14	6.25	3.44 (5.37)
6	1.5	0.83 (1.29)	15	2	1.10 (1.72)
7	0.5	0.28 (0.43)	16	8	4.40 (6.88)
8	2	1.10 (1.72)	17	2	1.10 (1.72)
9	0.67	0.37 (0.58)	18	12.5	6.88 (10.74)

Experimental Test Results

The HPFRC specimens, particularly the S1 column specimen, displayed enhanced ductile behavior and higher damage tolerance in comparison to the geometrically "identical" plain concrete Specimen BC. The HPFRC specimens developed relatively similar damage states as the reference BC specimen, but at higher displacement demands. At the maximum ductility demand level of 4.5 (3.9% drift) imposed on the BC specimen, the damage observed in both S1 and S2 HPFRC columns was smaller than that in the conventional concrete specimen, as seen in Figure

2. At this displacement level, while large portions of the BC column cover spalled off, the HPFRC columns had sustained relatively minor damage, and spalling had not occurred despite relatively large flexural cracks. The plastic hinge length in Specimen S1 was approximately 18" at the end of the test. The propagation of the plastic hinge zone with multiple cracking in the S1 column occurred from the center of the plastic hinge zone, estimated at a height of 14", upwards as well as towards the base of the column. The S2 column, nonetheless, presented a primary crack at a height of 10" above the foundation at the cut-off point of the dowel bars, resulting in a concentration of rotation and damage around that region and limited spreading of the plastic hinge zone towards the base of the column. The extension of the BC column plastic hinge zone was estimated at 12", equivalent to ¾ of the column diameter. Both HPFRC columns presented elastic behavior up to a drift ratio of approximately 1.3% (ductility of 1.5 in the BC column) No significant sliding (horizontal movement of the column across the plastic hinge region) was observed in the HPFRC specimens.

(a) (b) (c)

Figure 2. State of Specimens S1 (a), S2 (b), and BC (c) at the end of the cycle corresponding to a nominal ductility demand of 4.5 (3.9% drift).

The force-deformation response of the HPFRC and BC specimens is shown in Figure 3. Only the principal cycles at nominal displacement ductility levels of 1, 1.5, 2, 3, 4.5, 6.25, 8, and 12.5 (drift ratios of 0.86, 1.29, 1.72, 2.58, 3.87, 5.37, 6.88, and 10.7%) are presented. The deformation axis is expressed in terms of total drift ratio (displacement of the column top divided by the height from the column base to the actuator axes). The force axis is expressed in terms of total shear stress and shear ratio. The total shear stress was estimated as the total shear force divided by the effective area in shear, defined by Caltrans SDC (2004) as 0.8 times the gross area of the column. The total shear ratio was obtained by dividing the total shear force in the column by the assumed shear strength provided by the transverse steel reinforcement at yielding, estimated according to Caltrans SDC (2004). Figure 3 indicates an increased shear demand in the HPFRC specimens compared to the BC specimen due to the presence of dowels and the addition of fibers to the concrete mix. A wider gap in shear demand between the HPFRC and BC columns can be seen when shear is normalized by the contribution of the spiral reinforcement because of the 50% reduction in steel transverse reinforcement in the HPFRC columns. The peak shear ratio in the HPFRC columns was approximately three times higher than that in the BC specimen.

A comparison of HPFRC and BC specimen force-deformation response demonstrates the benefits of using HPFRC: Even though the shear demand on the HPFRC specimens increased significantly and the amount of transverse reinforcement was reduced by half compared to the BC specimen, the HPFRC specimens maintained a stable hysteretic behavior governed by flexure throughout the entire cyclic loading history. The addition of steel fibers to the concrete mix helped maintain high levels of shear strength at very large displacement ductility demands. The degradation of shear force with the progression of damage in the HPFRC specimens that initiated at a nominal displacement ductility of 6.25 (5.4% drift) was solely governed by the loss of flexural capacity (concrete crushing, bar buckling, and finally rebar fracture), not due to shear-related damage. Sliding or significant shear distortions were not evident, and no pinching (gap-like response) was visible in the hysteretic loops.

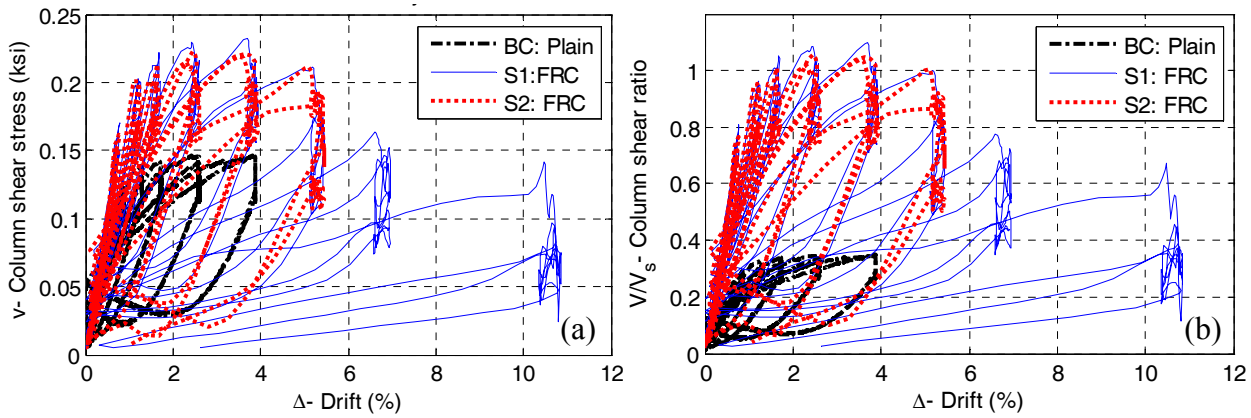

Figure 3. Hysteretic behavior of the HPFRC and BC specimens: (a) Total shear stress vs. total drift; and (b) Total shear ratio vs. total drift.

Calibrated Plastic Hinge Model

Biaxial rotation measurements along the column height were obtained from the instrumentation of relative vertical deformations on the face of the column at four six-inch segments extending from the column base to a height of 2 ft. These rotation profiles were converted to average curvature profiles and are plotted in Figure 4a, 4c, and 4d for Specimens S1, S2, and BC, respectively. S1 column developed an extensive plastic hinge zone with a length L_p of up to 18" (greater than one column diameter), with several circumferential cracks above and below what can be considered the center of the plastic hinge zone, estimated at a height of 14". Specimen S2, nonetheless, developed a single primary crack at a height of 10" above the foundation at the cut-off point of the dowel reinforcement, resulting in a concentration of rotation and damage around that region and limited spreading of inelastic deformations towards the base of the column. The extension of the BC column plastic hinge zone, which started at the column base level, was estimated at 12", equivalent to ¾ of the column diameter, thus presenting a more localized spreading of inelasticity in comparison to the S1 column.

The significant difference in the length of the plastic hinge zones among the three specimens shows that it is possible to design and detail the longitudinal reinforcement to achieve a highly desirable spreading of plastic deformation. In particular, the addition of dowel reinforcement elevated the center of the plastic hinge zone from the column base, thus providing more clearance for its spreading. Moreover, debonding of the dowel reinforcement (and thus

avoiding termination of dowels within the plastic hinge) in the S1 column allowed effective spreading of bar yielding along the plastic hinge region and the formation of several layers of flexural cracks in the HPFRC column. A less successful detail, used in Specimen S2, shows that there are significant unexplored opportunities to develop improved designs to enhance the deformation capacity of HPFRC plastic hinges. While the additional shear strength obtained by the use of steel fibers is helpful in developing a very deformable flexural plastic hinge, the adverse consequences of increased hoop spacing, particularly the reduction of buckling resistance of longitudinal reinforcing bars, should be explored. Also, the efficiency of HPFRC cover to provde support to the longitudinal bars should also be investigated.

The idealized curvature profile and a plastic hinge deformation model for the S1 column are presented in Figure 4b and Eq. 1, respectively. A similar equation (Eq. 2) was developed for column S2. In this model, the length of the plastic hinge zone, L_p, was set at 16" and 6" for Specimens S1 and S2, respectively, while the distance between the column base and the bottom the plastic hinge zone, h_{LP} was set at 6" for both HPFRC specimens. The resulting center of the plastic hinge zone coincided approximately with the middle of the debonded region in each column. The yield curvatures $\phi_{y,Top}$ and $\phi_{y,Bottom}$ were defined at a height of 22" (top end of the plastic hinge zone) and at the column base, respectively, from moment-curvature analyses of the top and bottom column segments of the corresponding HPFRC column, which have different longitudinal reinforcement ratios. An error of less than 10% was obtained in the computation of lateral deformations, u as a function of the nominal ductility, μ.

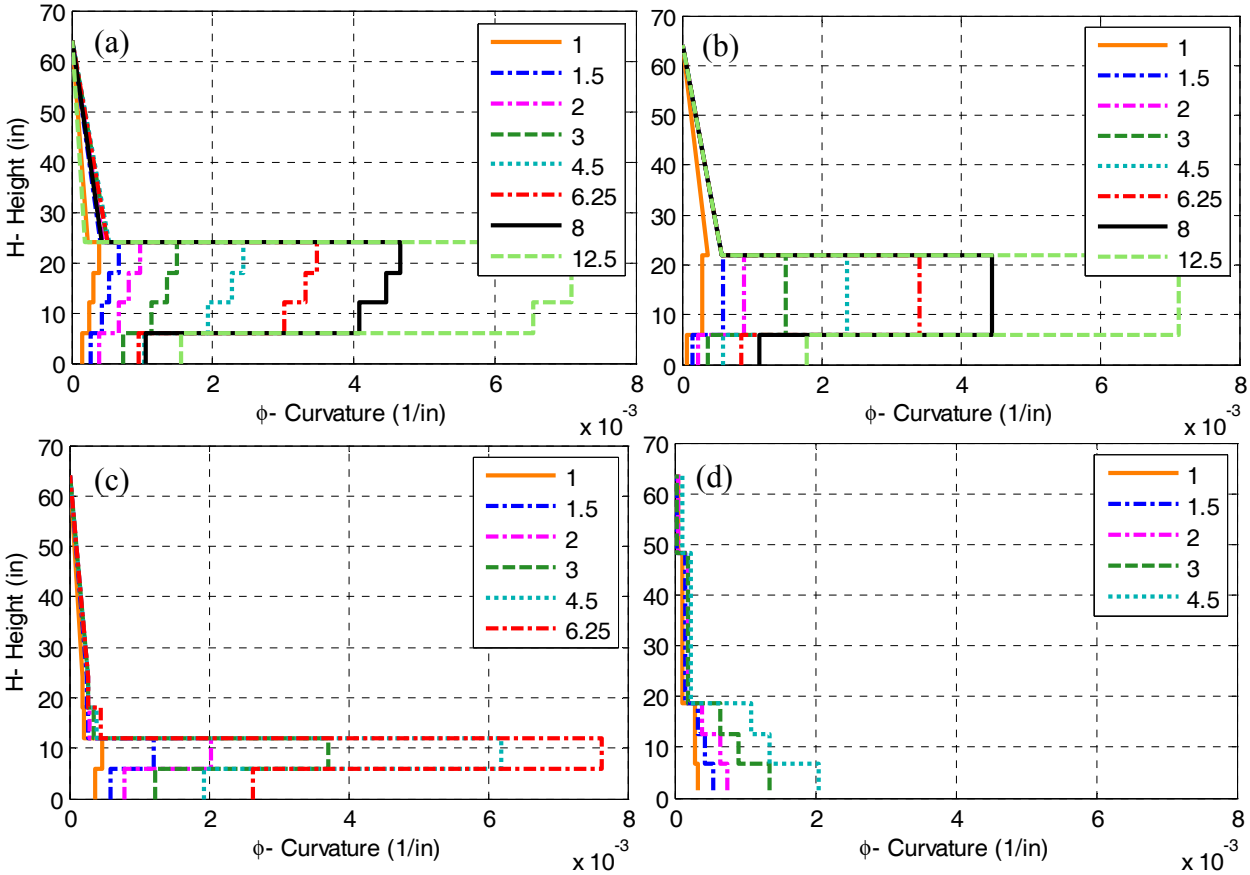

Figure 4. Curvature profiles for: (a) S1- Experimental results; (b) S1 - Calibrated plastic hinge model; (c) S2- Experimental results; and (d) BC- Experimental results.

$$\text{S1: } u(\mu) = \begin{aligned} &\phi_{y,Top} \cdot \min\left(1, \frac{\mu}{H_{Tot}} \cdot \left(H_{Tot} - L_p - h_{Lp}\right)\right) \frac{\left(H_{Tot} - L_p - h_{Lp}\right)^2}{3} + \ldots \\ &\phi_{y,Bottom}(\mu - 0.5) L_p \left(H_{Tot} - \frac{L_p}{2} - h_{Lp}\right) + \frac{\phi_{y,Bottom}}{4}(\mu - 0.5) h_{Lp} \left(H_{Tot} - \frac{h_{Lp}}{2}\right) \end{aligned} \quad (1)$$

$$\text{S2: } u(\mu) = \begin{aligned} &\frac{\phi_{y,Top}}{2H_{Tot}} \cdot \frac{\left(H_{Tot} - L_p - h_{Lp}\right)^3}{3} + \phi_{y,Bottom}(2.35\mu - 1.3) L_p \left(H_{Tot} - \frac{L_p}{2} - h_{Lp}\right) + \ldots \\ &\frac{\phi_{y,Bottom}}{4}(2.35\mu - 1.3) h_{Lp} \left(H_{Tot} - \frac{h_{Lp}}{2}\right) \end{aligned} \quad (2)$$

Peak Bond Stress in Dowel Reinforcement of HPFRC Specimens

The peak bond stress in the dowel bars of specimens S1 and S2 was computed from the peak strain profiles obtained using strain gage measurements. Assuming a minimum development length, L_d of 6" required to develop the full capacity of the rebar and an average uniform bond stress in the HPFRC material, u_b, along this development, the peak bond stress for bar strain values not exceeding yield strain was approximately $u_{b,\max} = 18\sqrt{f'_{c,FRC}}$ (psi). This value is significantly higher than typical bond strength developed in regular concrete: $12\sqrt{f'_c}$ (psi) and $6\sqrt{f'_c}$ (psi) for deformed bars with slip values smaller and larger than slip at rebar yield strain, respectively (Eligehausen *et al.* 1983).

Analytical Validation

A finite element model of a cantilever column was implemented and analyzed using OpenSystem for Earthquake Engineering Simulation (OpenSees) by Mckenna *et al.* (2000) to simulate the cyclic response of the HPFRC columns tested. The cantilever column was modeled in OpenSees using fiber cross-sections (*Fiber* section in OpenSees) and force-based formulated beam-column elements with distributed plasticity (*nonlinearBeamColumn* in OpenSees). Three elements were used along the column height to distinguish between the different longitudinal reinforcement details in the column base, unbonded region, and the column top segment. Five integration points were used for the top segment of the column and two integration points were used for the bottom two segments in the region of the plastic hinge zone. The HPFRC cover and core material behaviors were defined using the uniaxial *Concrete02* constitutive model in OpenSees with parameters defined according to material test results carried out for this study (Aviram *et al.* 2009). The *Hysteretic* constitutive model was used for the longitudinal steel of the HPFRC bridge columns, defined according to the calibrated OpenSees model of HPFRC columns by Aviram *et al.* (2009). The *Hysteretic* material model is defined with a tri-linear hysteretic behavior, pinching of force and deformation, damage due to ductility and energy, and degraded unloading stiffness based on ductility.

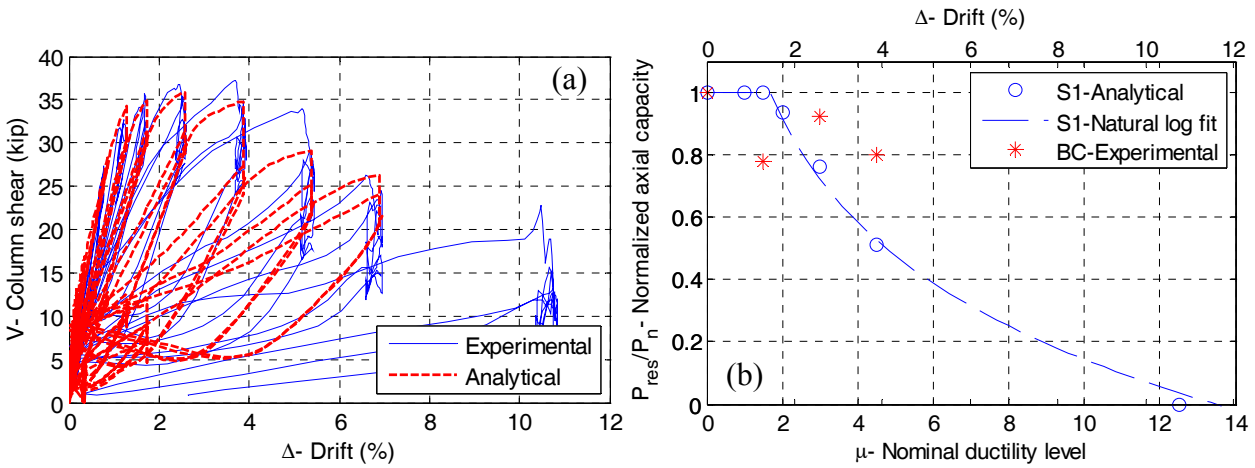

Figure 5. (a) Hysteretic loops of S1 column and OpenSees analytical model; (b) Degradation of residual axial capacity obtained with OpenSees model of S1 column.

The hysteretic loops relating total shear force to total drift ratio for the experimental and analytical results of S1 column are presented in Figure 5a. Using the calibrated analytical model, the peak strength and general shape of the hysteretic loops of Specimen S1 were successfully modeled up to the nominal ductility level of 8 (6.9% drift), after which significant damage occurred in the specimen invalidating modeling assumptions and making comparisons difficult. The calibrated analytical model of the S1 column was used to compute its residual gravity load carrying capacity following cyclic loading histories to different ductility demand levels. The residual concrete strength of the HPFRC cover and core constitutive models defined in OpenSees were based on cylinder testing results carried out for this study. Figure 5b presents the residual axial load capacity as a function of the nominal ductility demand for the analytical S1 column model, as well as the experimental results for BC specimen, tested up to a ductility demand of 4.5. Residual axial capacity degradation patterns of the S1 analytical model and the BC column specimens show a similar trend. Due to lack of additional experimental data for the BC specimen, the use of a similar fit relating its residual axial load and ductility demand levels could not be obtained with high confidence.

Conclusions

This paper presents the main experimental results obtained from highly demanding biaxial cyclic load tests of two approximately ¼-scale circular cantilever column specimens constructed using strain hardening, high-performance fiber-reinforced concrete (HPFRC) in comparison to a geometrically "identical" regular concrete specimen. The HPFRC column specimens were constructed using ready-mix concrete, adding the fibers to the concrete truck on site and by placing the HPFRC using a bucket and stick vibrators. The plastic hinge region of the specimens was detailed using relaxed transverse reinforcement, dowel reinforcement at the column base to prevent concentration of damage at the column-base interface, and debonding plastic sleeves intended to increase the spread of yielding and offset longitudinal steel fracture.

All column specimens presented a stable hysteretic behavior controlled by flexure with negligible shear-related damage; however, the HPFRC specimen with long dowels, S1, exhibited an extended plastic hinge zone with an approximate length of one column diameter, improved ductile behavior, high-damage tolerance, and high energy dissipation, in comparison to the

regular concrete specimen. This specimen was cycled up to a nominal ductility level of 12.5 (10.7% drift ratio), computed with respect to the regular concrete column yield point, while sustaining the applied gravity load. Even though the relocation of the plastic hinge region in the this specimen led to a substantial increase in plastic rotation demand for the same drift level, compared to the regular concrete column, the HPFRC material and the reinforcement detailing provided the necessary deformation capacity superior to that of conventional reinforced concrete.

The results of these unique tests demonstrate the advantages of HPFRC and call for additional research on the design and detailing of the plastic hinge region to best utilize the properties of HPFRC to achieve improved seismic performance and reduced post-earthquake repair costs of bridge structures. Furthermore, the use of HPFRC is expected to simplify the construction of critical regions in bridges, which require extensive reinforcement detailing resulting in rebar congestion and high construction difficulty.

References

Aviram, A., 2009. Structural Response and Cost Optimization in Bridge Construction using Performance Enhancement Strategies. Ph.D. Dissertation, University of California, Berkeley.

Caltrans, 2004. *Seismic Design Criteria 1.3*. California Department of Transportation, Sacramento, CA.

Canbolat, B.A., Parra-Montesinos, G.J., and Wight, J.K., 2005. Experimental Study on Seismic Behavior of High-Performance Fiber-Reinforced Cement Composite Coupling Beams, *ACI Structural Journal*, 102(1), 159-166.

Cheng, M.Y., and Parra-Montesinos, G.J., 2007. Punching Shear Resistance and Deformation Capacity of HPFRC Connections in Slab-Column Frames Subjected to Earthquake-Induced Displacement, *Proceedings of High Performance Fiber Reinforced Cement Composite 5 (HPFRCC5)*, edited by H.W. Reinhardt and A.E. Naaman, Mainz, Germany.

Harajli, M.H., and Rteil, A.M., 2004. Effect of Confinement Using Fiber-Reinforced Polymer or Fiber-Reinforced Concrete on Seismic Performance of Gravity Load-Designed Columns, *ACI Structural Journal*, 101(1): 47-56.

Mckenna, F., Fenves, G.L., Scott, M.H., and Jeremic, B., 2000. *Open system for earthquake engineering simulation*, http://opensees.berkeley.edu.

Parra-Montesinos, G.J., 2005. High-Performance Fiber-Reinforced Cement Composites: An Alternative for Seismic Design of Structures, *ACI Structural Journal*, 102(5), 668-675.

Parra-Montesinos, G. J., and Chompreda, P., 2007. Deformation Capacity and Shear Strength of Fiber-Reinforced Cement Composite Flexural Members Subjected to Displacement Reversals, *Journal of Structural Engineering*, 133(3), 421-431.

Terzic. V, Mackie, K., and Stojadinovic, B., 2008. Experimental Evaluation of the Residual Axial Load Capacity of Circular Bridge Columns, *Proceedings of the 14th World Conference on Earthquake Engineering*, Beijing, China.

Yoon, J.K., Billington, S.L., and Rouse, J.M., 2002. Precast Segmental Bridge Piers with Unbonded Post-tensioning and Ductile, Fiber Reinforced Concrete for Seismic Applications, *Proceedings of the 7th National Conference of Earthquake Engineering (NCEE)*, Boston.